

MCMAG: A COMPUTER PROGRAM TO SIMULATE MAGNETIC STRUCTURES

P. LACORRE^{1,2} and J. PANNETIER¹

¹ Institut Laue–Langevin, Avenue des Martyrs, 156X, 38042 Grenoble Cedex, France

² Laboratoire des Fluorures, UA449 Université de Maine, Route de Laval, 72017 Le Mans Cedex, France

Received 21 July 1987

MCMAG is a Fortran program based upon a Monte Carlo algorithm to simulate magnetic models from postulated coupling constants. Any kind of 3D periodic model as well as real magnetic structure can be simulated without limitation of interaction distance. The spin Hamiltonian contains a two spin coupling term of Heisenberg type, a single ion anisotropy term and an applied field term. MCMAG can be used as a tool to study the temperature and field behaviour of complex magnetic models; real magnetic structures can also be reproduced, as well as peculiar dynamic effects and magnetic transitions under applied field. The program provides facilities to determine (H, T) phase diagrams.

1. Introduction

The numerical technique known as Monte Carlo is extensively used in statistical physics (see for instance refs. [1–3]). Initially introduced by Metropolis et al. [4] for a study of the equation of state of liquids, the method has spread to a broad range of application in physics and has been particularly fruitful in the field of magnetic systems. Most of these studies have been devoted to investigation of phase transitions and critical phenomena, most often on simple model systems (cubic lattices, frustrated triangular lattice...). In this paper, we shall concentrate on a different, more experimentalist-directed approach; indeed Monte Carlo simulation can readily contribute at elucidating and understanding the magnetic behavior of “real” complex magnetic materials and thereby be a useful tool to investigate magnetic ordering in solids. The aim of this paper is to describe a “general purpose” program for Monte Carlo simulation of magnetic models and illustrate some of its applications.

The presentation of this paper is as follows: in section 2 we briefly recall the basic features of the Monte Carlo and simulated annealing techniques and give a general description of the program. Some applications of the program are presented in

section 3: this includes the simulation of magnetic models, the prediction of magnetic structures, the simulation of induced transition under applied field and of thermal behaviour in some peculiar magnetic materials. In the last section, we shall briefly examine applications and possible future extensions of the program.

2. Methodology

2.1. Algorithm

The algorithm used in the program MCMAG is based upon the Metropolis “importance sampling” method [4]. Details about the theoretical grounds of the algorithm can be found in ref. [2] for instance. From a technical point of view, the method can be summarized as follows: consider a system of n spins in interaction, each spin i ($i = 1, n$) with the orientation S_i . The interaction energy of the system may be written $E = f(S_1, S_2, \dots, S_i, \dots, S_n)$. The aim of the method is, knowing the function f (which will be defined below), to minimize E by adjusting the orientations S_i in such a way as to determine the ground state of the system. In the program, the spins are examined one after each other and their possible

new orientation randomly determined. If the new orientation of the spin lowers the energy of the system, it is accepted. If it increases the energy, the new orientation is not systematically rejected: an occurrence probability p is affected to the transition, where p is defined by $p = \exp(-(E_1 - E_0)/kT)$. This probability is similar to a Boltzmann factor, T being assimilated to the temperature (k is a scale factor). The low temperature equilibrium is reached by simulated annealing [5]: during the process, T is slowly decreased and, if this annealing is performed slowly enough, the spin configuration which is frozen will correspond to the ground state configuration of the system. Thus the successive steps of the calculation are as follows:

- generate a system of n randomly orientated spins $S_1^0, S_2^0, \dots, S_n^0, \dots, S_n^0 \Rightarrow$ energy E_0 and define an initial value of temperature T_0
 - select a spin S_i^0 among the n spins
 - propose a new randomly determined orientation $S_i^1 \Rightarrow$ new energy E_1
 - calculate $p = \exp[-(E_1 - E_0)/kT_0]$
 - draw a random number Nr ($0 \leq Nr < 1$)
 - if $Nr \leq p$ the new orientation S_i^1 is adopted
 - if $Nr > p$ the previous orientation S_i^0 is preserved
 - select a new spin
- internal loop

This loop is executed n times in such a way as to examine every spin in the sample box. These n loops form what is called one Monte Carlo cycle. A large number of Monte Carlo cycles (say a few thousand) is usually necessary to reach a stable configuration. Then a new temperature $T < T_0$ is fixed and the above process is repeated until a new equilibrium is reached. The calculation is stopped when no appreciable change in the spin configuration is noticed.

2.2. Hamiltonian

The Hamiltonian used for the calculation of the energy E (i.e. the function f mentioned above)

may take various forms depending on the assumed coupling. We have chosen the simplest and more general form commonly accepted for the spin coupling. This spin Hamiltonian (see for instance ref. [6]) in the present version of the program includes three terms:

- a coupling term:

our convention for the coupling constants is the following: J is taken negative for an antiferromagnetic coupling. The two spin coupling Hamiltonian is defined by $H = -\sum_{\langle i,j \rangle} J_{ij} \mathbf{S}_i \cdot \mathbf{S}_j$ where $\langle i, j \rangle$ represents the summation over the pairs of spins of the system. The spins \mathbf{S}_i have three degrees of freedom (Heisenberg type). A possibility for anisotropic coupling constants has been introduced.

- a single-ion anisotropy term:

for each spin i this term is defined as $D_i(\mathbf{r}_i \cdot \mathbf{S}_i)^2$ where D_i is the anisotropy coefficient and \mathbf{r}_i the direction of the anisotropy.

- an applied field term:

if an external magnetic field is applied, one must include an additional term defined by $-\sum_{i=1}^n \mathbf{H} \cdot \mathbf{S}_i$ where \mathbf{H} is the applied field.

Thus the more general form of the energy used in the program is:

$$E = - \sum_{\langle i,j \rangle} \sum_{\alpha} J_{ij}^{\alpha} S_i^{\alpha} S_j^{\alpha} + \sum_{i=1}^n D_i (\mathbf{r}_i \cdot \mathbf{S}_i)^2 - \sum_{i=1}^n \mathbf{H} \cdot \mathbf{S}_i \quad \text{where } \alpha = x, y, z.$$

A 2D version of the program with planar XY spins is available, as well as a 3D Ising version.

2.3. General structure of the program

The program has been written to simulate the magnetic ordering and the behaviour under an applied field of any 3D cluster and 3D periodic structure.

A structure is described by a so-called basic unit cell (b.u.c.), which can be the crystallographic unit cell but not necessarily. The sample used for simulation can be built up from one or more b.u.c. The boundary conditions may be of three types: free boundary conditions, periodic boundary conditions or mixed boundary conditions (a combina-

tion of free and periodic boundary conditions). Magnetic interactions are not limited to the nearest neighbours and may be established between any pair of magnetic atoms of the structure. The input of the sample size and external parameters of the simulation (cooling or heating rate, magnetic field, number of Monte Carlo cycles) is done interactively. The conversational mode has been worded with enough flexibility to allow an easy shift within the (H, T) plane for determination of magnetic phase diagrams.

The data relative to the b.u.c. are stored in an input file. It contains the topology of the system, the values of magnetic interactions, anisotropy coefficients and spin amplitudes. One has to point out that the approach is essentially topological. By no means crystallographic positions are taken into account by the program. Every magnetic atom is assumed to be independent: no symmetry element is introduced in the program. If symmetries appear in the ground state configuration of spins, they are only a consequence of parity in coupling constant values. The structure is built up from the stacking of unit cells along the crystallographic axes. The coordinates of any unit cell relative to the basic unit cell are obtained by a simple index-

ing along these axes (coordinates of the b.u.c. = $(0, 0, 0)$). The NA atoms of the b.u.c. are numbered from 1 to NA. Every atom has NV neighbours which are located either inside the b.u.c. or in a neighbouring cell. Every neighbour is identified by its number in the b.u.c. and by the indexing of its unit cell. A spin of the desired amplitude is allocated to every atom.

A detailed description of an input file is given in appendix A. As a simple illustration, the input file concerning the kagomé layer with antiferromagnetic interactions between nearest neighbours only (see fig. 1) is provided in table 1. Technical details concerning the program are given in appendix B.

2.4. Output

The random spins are set up by a random generator of points located at the surface of a sphere of radius equal to the saturated magnetic moment. After N_c Monte Carlo cycles at the actual temperature, the value and direction of spin attributed to each atom correspond to the mean of the successive configurations of the spin during these cycles. In fact equilibrium is not reached

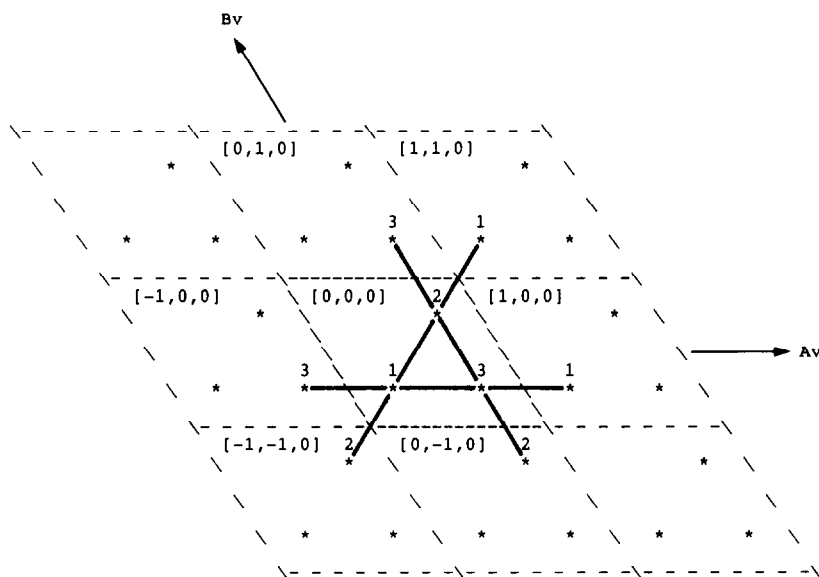


Fig. 1. The kagomé layer with atom numbering and cell indexing as used in the program MCMAG (see table 1). Nearest neighbour interactions have been drawn (full lines).

Table 1
Example of input file for MCMAG: kagomé layer with interactions between first neighbours only (fig. 1) *

TITLE CARD	kagomé layer interactions between first neighbours only							
DEFINITION CARD	3	0	3					
ATOM CARD	1	4	10	0	0	1		
INTERACTION CARDS	⎧		2	0	0	0	-10	
			3	0	0	0	0	-10
			2	-1	-1	0	0	-10
ATOM CARD	⎨		3	-1	0	0	-10	
			1	0	0	0	0	-10
			3	0	0	0	0	-10
INTERACTION CARDS	⎧		1	1	1	0	-10	
			3	0	1	0	0	-10
			1	0	0	0	0	-10
ATOM CARD	3	4	10	0	0	1		
INTERACTION CARDS	⎧		1	0	0	0	-10	
			2	0	0	0	0	-10
			1	1	0	0	0	-10
SPIN CARD	1	3	5					
CELL CARD	8.	8.	4.	90	90	120		

* The amplitude of spins are set to $5\mu_B$. The anisotropy coefficients are set to $+10$ K along the $[0\ 0\ 1]$ direction in order to constraint the spins to lie in the (a, b) plane.

immediately and some thermalization sweeps are allowed before the mean values calculation which is performed during the Nc–Nd last cycles (Nc and Nd are fixed by the user). The output of spin configuration consists in the projection of the mean spins on the axis of the orthogonal reference coordinate system, and the standard deviation calculated from the spin fluctuations during the Nc–Nd cycles. Projection of the spins on the crystallographic axes may be collected, as well as the rotation of the whole system in order to align a particular spin along a given direction.

Total magnetization of the sample is calculated, and also statistical values such as specific heat and magnetic susceptibility according to the formula [7]:

$$C = (\langle E^2 \rangle - \langle E \rangle^2) / kT^2,$$

$$\chi = (\langle M^2 \rangle - \langle M \rangle^2) / kT,$$

where $\langle E \rangle$ and $\langle M \rangle$ are the mean value of the energy and the magnetization of the system, respectively. These values are stored in an output file for further analysis or plotting.

3. Results

3.1. Simulation of magnetic models

3.1.1. Periodic models

An interesting feature of the program is its ability to simulate any kind of 2D or 3D periodic magnetic model without any limitation of distance between interacting neighbours. As a simple illustration, we show the results of a calculation on a classical triangular planar XY model with interactions between nearest and next nearest neighbours (noted, respectively, J_1 and J_2). Katsura et al. [8] have investigated analytically this system; they determined the phase diagram in the J_1 – J_2 plane and pointed out the appearance of a helimagnetic ordering inside a defined range (J_1, J_2). Fig. 2 shows the spin configuration which we obtained using a sample of 400 spins with $J_1 = +4$ and $J_2 = -16$, compared with the analytical result for $J_1/J_2 = -1/4$ as presented by Katsura. We used for the simulation a relatively slow cooling rate from $T = 100$ to $T = 0.4$ with 0.92 as a multiplicative coefficient, performing only 350 Monte Carlo cycles per spin at each temperature. The simulated helix screw is identical to the analytical result. We notice the slight distortion at the edges of the sample due to the free boundary conditions.

3.1.2. Cluster models

The program is also well suited to simulate spin arrangement of 3D clusters of magnetic atoms. As an example, we have simulated the spin configuration of magnetic atoms located at the vertices of an icosahedron, correlated by identical antiferromagnetic interactions between nearest neighbours only. The result is presented in fig. 3. For sake of clarity, we have reoriented the whole system in order to align one spin (spin 11 in the figure) along the corresponding diagonal of the icosahedron. But it is obvious that, without anisotropy, every spin is equivalent to each other.

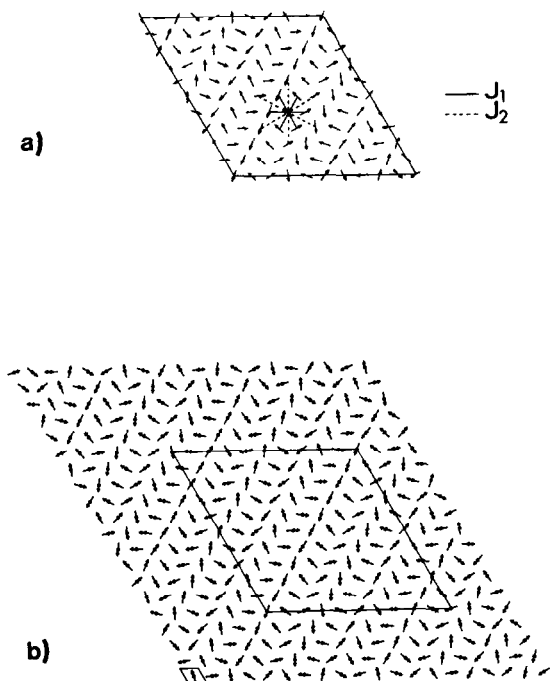


Fig. 2. (a) Ground state configuration of the triangular planar XY model with $J_1/J_2 = -1/4$ and $J_1 > 0$: analytical result (after ref. [8]); (b) result of the Monte Carlo simulation for a sample of 400 spins (20×20) with $J_1 = 4$ and $J_2 = -16$. Experimental parameters: cooling rate 0.92 from $T=100$ to $T=0.4$ with 350 MC cycles per spin at each temperature; free edges.

The main results of the simulation are the following:

- the two spins of any diagonal are arranged antiferromagnetically: the center of the icosahedron is a prime inversion center $\bar{1}'$,
- two neighbouring spins make an angle of about 116° (the exact value would be 116.57° , which is the dihedral angle of the dodecahedron). Second neighbours make an angle of 63.43° , the subtended angle of the icosahedron.

3.2. Prediction of magnetic structures

The input facilities of the program allow to simulate models with non-trivial topology and interactions, i.e. real magnetic structures. Then the problem is to evaluate the main coupling constants inside the compound which would be simulated. Except when direct or indirect measure-

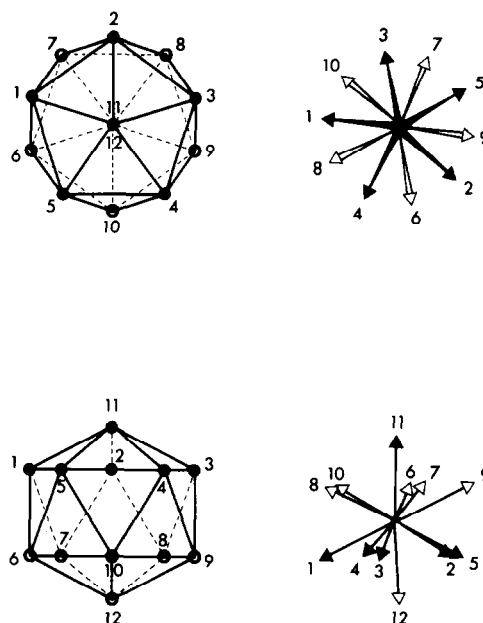


Fig. 3. Result of the Monte Carlo simulation of an icosahedral cluster with antiferromagnetic interactions between nearest neighbours. Projection along the 5-fold axis (top) and perpendicular to this axis (bottom).

ments have already been done on the compound itself, two approaches are possible to estimate the value of the coupling constants: experimental data from similar compounds and theoretical estimate. Among the last category, semi-empirical rules such as Kanamori–Goodenough rules [9,10], as well as model calculations (see for instance refs. [11–16]) may be considered.

An important point in simulating magnetic structures is the choice of the sample box and boundary conditions: it is actually crucial for prediction. A thoughtless choice of small sample with periodic boundary conditions may lead, in some cases, to unwanted strong magnetic constraints and therefore to totally inadequate results. To avoid this risk, a sensible procedure consists in using large samples and free edges boundary conditions. This ought to be the general method if the real magnetic cell is unknown. To save calculation time an intermediate procedure is to work with medium size samples (typically multiple of two and three times the crystallographic cell) and periodic boundary conditions, but it precludes a priori

the possibility of incommensurate or helimagnetic arrangement. If the magnetic cell is known experimentally, a convenient choice is of course the magnetic cell itself. With such very small samples, the algorithm converges very quickly to the solution.

The program has been tested on many known magnetic structures and a few examples are presented below. A first example is the fluoride $\text{Ba}_2\text{Ni}_3\text{F}_{10}$. It crystallizes in the monoclinic space group $P2_1/c$ with the following parameters (at room temperature): $a = 18.542 \text{ \AA}$, $b = 5.958 \text{ \AA}$, $c = 7.821 \text{ \AA}$, $\beta = 111.92^\circ$, $Z = 4$ [17]. Its magnetic structure as determined by neutron diffraction [18] is shown in fig. 4a. The magnetic cell is twice the crystallographic one (doubling of the c axis). In a first approximation we will assume that the main magnetic interactions in this compound take place between nearest neighbours only. The value of the coupling constants in $\text{Ba}_2\text{Ni}_3\text{F}_{10}$ can be estimated from those determined in other nickel fluorides with similar Ni–F–Ni superexchange angles, i.e. 180° , 130° and 95° . Such configurations are encountered in fluorides like NiF_2 [19], KNiF_3 [20], RbNiF_3 [21] or K_2NiF_4 [22] for which exchange interactions have previously been measured. From these results, the coupling constants in $\text{Ba}_2\text{Ni}_3\text{F}_{10}$ can be estimated as $J_1(95^\circ)/k = +8 \text{ K}$, $J_2(130^\circ)/k = -20 \text{ K}$ and $J_3(180^\circ)/k = -100 \text{ K}$. These values imply magnetic frustration inside square platelets (underlined in fig. 4a) for which the frustration function Φ_k [23] is negative. It is reasonable to assume that the strongest constraint within platelets takes place at the weakest interaction. Effectively the spin arrangement is antiferromagnetic whilst the coupling constant between nickel inside edge-sharing octahedra is expected to be ferromagnetic.

In order to test the validity of this argument, we performed a Monte Carlo simulation of the magnetic structure of $\text{Ba}_2\text{Ni}_3\text{F}_{10}$ using the above values of coupling constants. In absence of a priori information about the easy axis of magnetization in the compound, we only assigned a positive D anisotropy coefficient along the b axis of the structure (rutile chains) by comparison with NiF_2 . At this point, it is worth mentioning that the Hamiltonian does not contain any magneto-crys-

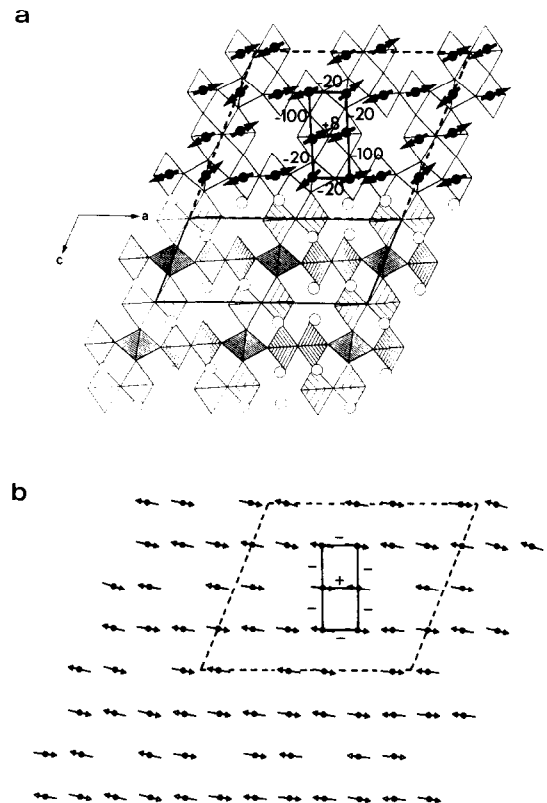


Fig. 4. (a) Magnetic structure of $\text{Ba}_2\text{Ni}_3\text{F}_{10}$ as determined by neutron diffraction [18]. Frustrated square platelets are indicated (heavy lines) together with a rough estimate of coupling constants; (b) result of the Monte Carlo simulation of the magnetic structure of $\text{Ba}_2\text{Ni}_3\text{F}_{10}$ using the previous coupling constants (no easy axis of magnetization was applied).

talline energy term; as a consequence, the minimization process will provide the coupling mode of spins but not their absolute orientation with respect to the chemical cell: this information is however sufficient to start the refinement of the magnetic structure from neutron diffraction data. As mentioned above, the choice of the sample box may be critical in some cases. Two approaches were possible to simulate $\text{Ba}_2\text{Ni}_3\text{F}_{10}$: the first one was to take advantage of the fact that the real magnetic cell exhibits a doubling of the c axis with respect to the crystal cell and choose the corresponding sample size with periodic boundary conditions; the second one was to proceed as if the magnetic cell was unknown, using a larger

sample with free edges boundary conditions. Both approaches have been tested and yield exactly the same results, which are presented in fig. 4b. The main features of the magnetic structure of $\text{Ba}_2\text{Ni}_3\text{F}_{10}$ are well reproduced:

- doubling of the c axis in the magnetic cell,
- collinearity of spins,
- antiferromagnetic arrangement of spins connected by ferromagnetic interactions inside square platelets,
- coupling modes.

Therefore, the assumption on the coupling constants in $\text{Ba}_2\text{Ni}_3\text{F}_{10}$ is in good agreement with the neutron diffraction results, in spite of the unexpected arrangement of spins.

Many magnetic compounds undergo internal magnetic constraints which force them to adopt non-collinear spin arrangement. This occurs for instance when magnetic ions in antiferromagnetic interaction are located on a triangular lattice. These competitions between interactions lead in high symmetry cases (typically hexagonal cells) and Heisenberg type spins to a 120° star configuration of spins (see for instance refs. [24–26]). Lower symmetry structure provide the opportunity to break the intrinsic equivalence of interactions and lead to a departure from the ideal 120° arrangement. This is the case for the chromium potassium fluoride $\alpha\text{-KCrF}_4$ which is built up from infinite columns of three corner sharing $[\text{CrF}_6]$ octahedra (fig. 5a) [28,29]. The magnetic structure inside basic triangular platelets [27] is no longer a 120° configuration (fig. 5b, N.D.). Superexchange angles which determine coupling constants in this compound, as shown in fig. 5a, are the following (room temperature, from refs. [28,29a]): $\alpha = 144.6^\circ$, $\beta = 140.2^\circ$, $\gamma = 149^\circ$. It has been shown [30] that superexchange coupling constants between two magnetic ions (M) inside corner sharing anion (X) octahedra have a linear dependence on $\cos^2\theta$ where θ is the superexchange angle M–X–M. Thus in KCrF_4 the distribution of superexchange angles would be responsible for slightly unbalanced coupling constants which could be the cause of the departure from ideal 120° configuration of spin. Unfortunately the lack of experimental data concerning coupling constant between Cr^{3+} ions by superexchange path via

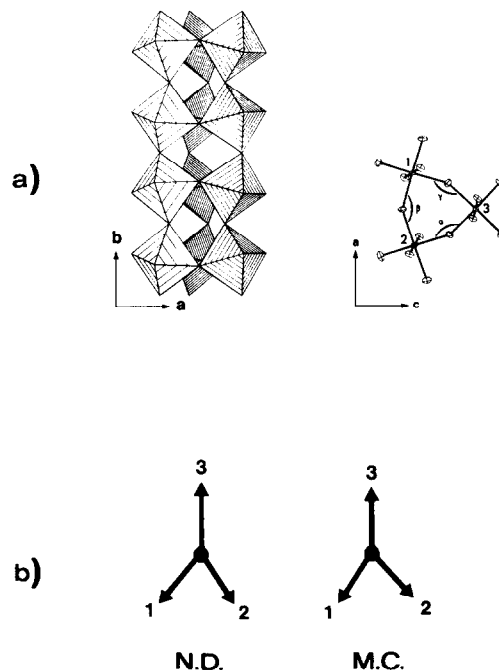


Fig. 5. (a) Views of an infinite triangular column of $[\text{CrF}_6]$ octahedra in $\alpha\text{-KCrF}_4$ ([27] from ref. [29]); (b) spin arrangement inside a triangular platelet of KCrF_4 (N.D.) compared with the result of Monte Carlo simulation assuming the coupling constants given in the text (M.C.).

various Cr–F–Cr angles prevents the kind of approach we used above for the barium nickel fluoride. However, the Kanamori–Goodenough rules at least provide quite firm presumption about the sign of 90° and 180° interactions, which should be ferromagnetic and antiferromagnetic, respectively [9,10]. With such limited information, only qualitative results may be expected; they tend to suggest that the departure from ideal spin configuration in KCrF_4 is mainly due to the unequivalent superexchange angles. The Monte Carlo simulation has been done with the assumption that $J_{90^\circ} = +7$ K and $J_{180^\circ} = -10$ K, fairly reasonable values with respect to Kanamori–Goodenough rules (however only coupling constant ratios must be thought to have any significance for these calculations). A linear dependence of the coupling constants with $\cos^2\theta$ leads in this case to the formulation $J_\theta = 7 - 17 \cos^2\theta$, i.e. $J_\alpha = -4.30$ K, $J_\beta = -3.03$ K and $J_\gamma = -5.49$ K. Starting

from these values, the result of simulation is in fair agreement with the neutron diffraction result, with a small angle (between spins 1 and 2) and two larger angles (fig. 5b).

We have however to emphasize the sensitivity of spin arrangement to small variation of coupling constants: an otherwise similar simulation with the assumption of $J_{90^\circ} = +10$ K and $J_{180^\circ} = -10$ K yields to a collinear magnetic structure with spins 1 and 2 parallel. When frustrated interactions are almost equal, slight departure from equivalence may imply significantly different spin orientations.

In order to simulate the helimagnetic ordering which often needs large unit cell dimensions, we have introduced a new type of boundary conditions that we have called mixed boundary conditions: they correspond to free boundary conditions along one direction (typically the screw axis of the helix) and periodic boundary conditions for the other two directions. The use of these boundary conditions obviously implies that the screw axis of the helix is already known (or assumed).

We have tested these boundary conditions by simulating the magnetic structure of the rutile β - MnO_2 , which is described as ordering helimagnetically below 84 K with a periodicity of $7c/2$ [31,32]. The rutile structure is presented in fig. 6a with the three main exchange integrals called J_1 , J_2 and J_3 . These have been measured to be equal to -8.8 , -5.5 and 1.3 K, respectively [33].

The magnetic structure of β - MnO_2 has been simulated assuming these coupling constant values on a sample containing $3 \times 3 \times 21$ cells, i.e. 378 atoms (2 atoms per cell), with the c direction as screw axis. The free edges boundary condition was applied along this direction, keeping the two others under periodic conditions (fig. 6b). The result of simulation is presented in fig. 7 (only the spin of the central column, i.e. cells $(2, 2, n)$, are drawn). The periodicity of the helimagnetic structure of β - MnO_2 is thus exactly reproduced. Free edges seem to have very little effect, except for the spins of edge cells themselves. At this stage, it is worth mentioning that a very important parameter to simulate large size samples is the cooling rate. Fig. 7 illustrates this point by showing the results of

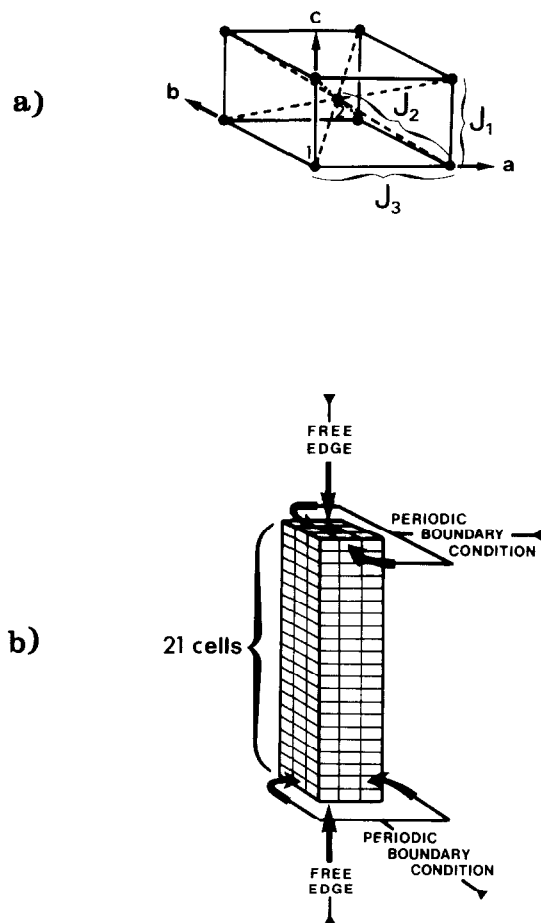


Fig. 6. (a) The rutile structure of β - MnO_2 (cationic lattice only) with indication of the three main coupling constants; (b) a perspective view of the sample ($3 \times 3 \times 21$ cells) used for the Monte Carlo simulation of β - MnO_2 together with special boundary conditions (the result of the simulation is presented in fig. 7).

two simulations performed with different cooling rates. The fastest annealing (right hand side figure) leads to the occurrence of two chirality domains with a grain boundary (commonly encountered in real helimagnetic compounds [34]) while a magnetic monodomain has grown from the slower one.

These examples show that MCMAG is an appropriate tool to simulate any kind of magnetic structure when coupling constants are known or, at least, can be roughly estimated. A straightforward application is to assist the determination of magnetic structures.

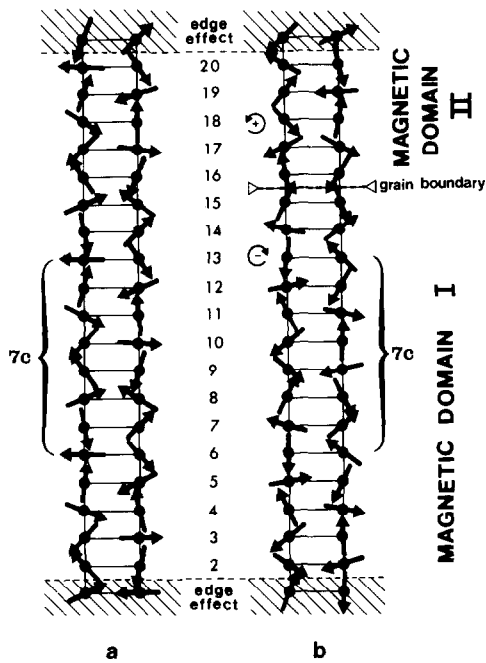


Fig. 7. Monte Carlo simulation of the helimagnetic structure of β - MnO_2 on a sample of 378 atoms ($3 \times 3 \times 21$ cells): projection on the (a, b) plane. Only the central column is drawn (cells with indexation (2, 2, n)). The coupling constants are taken from reference [33]. Experimental parameters: (a) cooling rate 0.92 from $T = 300$ to $T = 0.5$ with 3000 MC cycles per spin at each temperature and mixed boundary conditions; (b) cooling rate 0.90 from $T = 300$ to $T = 0.5$ with 1500 MC cycles per spin at each temperature and mixed boundary conditions.

3.3. Estimation of exchange integrals

The second example of the previous section has shown that the spin orientation may be extremely sensitive to small changes of coupling constants. This suggests the possibility of evaluating coupling constants in compounds with canted magnetic structure. This approach is in some respect the reverse of the previous one: starting from the magnetic structure as determined from neutron scattering experiments one tries to evaluate exchange constants in order to obtain a simulated spin arrangement as close as possible to the experimental one (in fact only ratios of coupling constants are reachable). We have undertaken this kind of evaluation for the fluoride $\text{MnFeF}_5 \cdot 2\text{H}_2\text{O}$; its crystallographic structure, which is of the in-

verse weberite type [35], is illustrated in fig. 8a. The compound is ferrimagnetic; its magnetic structure has been refined from neutron scattering experiment. The results are presented in table 2 N.D. [36,37]. There are 8 cations (4 Mn + 4 Fe) in the magnetic cell. The modes of coupling are ferromagnetic for the x-component of the moments (F_x) and antiferromagnetic for the z-component of the Fe^{3+} moment (G_z). We shall assume that the stronger interactions take place between nearest magnetic neighbours, through M-F-M superexchange path. The canted magnetic structure (fig. 8b) is thought to be a consequence of magnetic constraints inside the triangular platelets (underlined in the figure) involving two Fe^{3+} and one Mn^{2+} : according to Kanamori-Goodenough rules, 180° d^5 - d^5 superexchange coupling constants are expected to be antiferromagnetic, thus leading to a negative frustration function inside the platelets, i.e. to the occurrence of magnetic frustration. $\text{MnFeF}_5 \cdot 2\text{H}_2\text{O}$ exhibits two types of nearest neighbours interactions: $J_{\text{Fe-Fe}}$ and

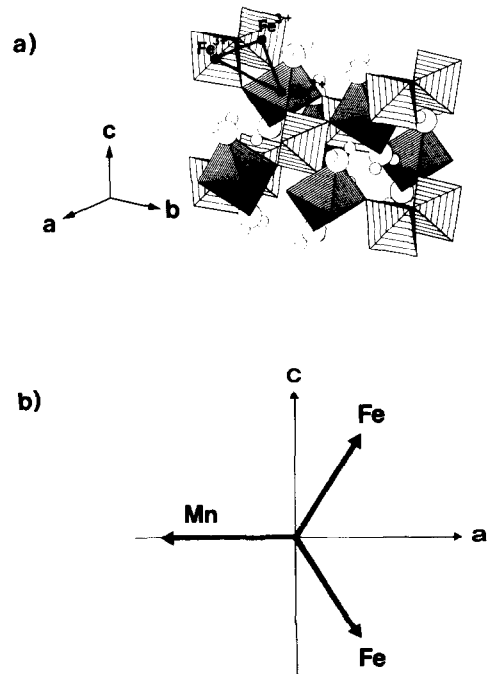


Fig. 8. (a) Crystal structure of $\text{MnFeF}_5 \cdot 2\text{H}_2\text{O}$ [38]: a frustrated triangular platelet is outlined; (b) spin arrangement inside a triangular platelet of $\text{MnFeF}_5 \cdot 2\text{H}_2\text{O}$ [37].

Table 2

Results of Monte Carlo simulation (MC) of the magnetic structure of $\text{MnFeF}_5 \cdot 2\text{H}_2\text{O}$ with $J_{\text{Mn-Fe}}/J_{\text{Fe-Fe}} = 0.492$ compared with the neutron diffraction refinement (N.D.) [37]

	Atom	Mn(1)	Mn(2)	Mn(3)	Mn(4)	Fe(5)	Fe(6)	Fe(7)	Fe(8)	Total mag.
M.C.	M_x	-4.260	-4.268	-4.271	-4.260	2.045	2.204	2.175	2.006	2.157 $\mu_{\text{B}}/\text{mol}$
	M_y	-0.054	-0.132	-0.059	-0.090	-0.109	0.211	0.108	0.033	
	M_z	-0.063	-0.110	-0.058	-0.038	3.375	-3.260	-3.293	3.401	
	total M (μ_{B})	4.261	4.272	4.271	4.262	3.948	3.941	3.948	3.949	
N.D.	M_x	-4.29	-4.29	-4.29	-4.29	2.13	2.13	2.13	2.13	2.16 $\mu_{\text{B}}/\text{mol}$
	M_y	0	0	0	0	0	0	0	0	
	M_z	0	0	0	0	3.35	-3.35	-3.35	3.35	
	total M (μ_{B})	4.29	4.29	4.29	4.29	3.97	3.97	3.97	3.97	

$J_{\text{Mn-Fe}}$. Our aim was to determine the ratio $J_{\text{Mn-Fe}}/J_{\text{Fe-Fe}}$ in this compound.

In the magnetic structure, the spins lie in the (a, c) plane and the moments of Mn^{2+} cations are aligned along the a axis. To reproduce this feature, we have assigned a positive D anisotropy coefficient along the b axis to Fe^{3+} spins (in order to constraint them to lie in the (a, c) plane) and a negative D coefficient along a axis to Mn^{2+} spins (to align them along a). However, these coefficients do not add further constraints on frustrated platelets: they only allow direct comparison of the results with the real magnetic structure. We have arbitrarily fixed the $J_{\text{Fe-Fe}}$ constant to -6 K, a reasonable value for 180° $\text{Fe}^{3+}\text{-F-Fe}^{3+}$ superexchange, and adjusted, by trial and error, the $J_{\text{Mn-Fe}}$ constant in order to reproduce the experimental spin direction. Spin amplitude was fixed to saturated magnetic moments as determined by neutron diffraction at low temperature, i.e. $3.97\mu_{\text{B}}$ for Fe^{3+} and $4.29\mu_{\text{B}}$ for Mn^{2+} . The best result (see table 2 M.C.) was obtained for $J_{\text{Mn-Fe}}$ coupling constant equal to -2.95 K. From this result, we are able to estimate the ratio $J_{\text{Mn-Fe}}/J_{\text{Fe-Fe}}$ in $\text{MnFeF}_5 \cdot 2\text{H}_2\text{O}$ as $2.95/6 = 0.49$ (remanent magnetization of both Monte Carlo simulation and neutron diffraction refinement are in good agreement with measurement under applied field [38,39]).

This example shows that coupling constant ratios can reasonably well be estimated using this

program especially in case where the magnetic structure is non-collinear and when it can be assumed that a limited number of strong interactions occur in the solid.

3.4. Dynamical behaviour under applied field

This section is concerned with the possibilities offered by the program to study the influence of magnetic field on magnetic structures, mainly antiferromagnetic structures which provide the richest range of behaviour. As a matter of fact it is well known (see for instance ref. [40] and references therein) that a magnetic field applied along the easy magnetization axis of an antiferromagnetic substance induces a reorientation of spins called metamagnetic or spin-flop transition. The program gives the possibility to study this behaviour on any kind of model.

First we shall examine the result of simulation concerning models which have already been studied analytically in the literature. Let us begin with a chain of Heisenberg spins in antiferromagnetic interaction. This elementary model provides a good illustration of the spin-flop transition which corresponds to the abrupt reversal of the two AF sublattices of spins perpendicularly to the field at a critical field H_c . The two orientations of spin make an angle which progressively decreases in an increasing field until saturation which occurs at a higher field H_0 . The occurrence of metastable

states near the spin-flop transition is responsible for hysteresis at the transition when increasing and decreasing fields are applied [41]. If the anisotropy of the system is strong compared to the exchange, the spin-flop mechanism is replaced by another one, the metamagnetic transition, which is the direct reversal of one sublattice parallel to the other. We present below the case of a moderately anisotropic system. The scaling stiffness energy of such a 1D anisotropic Heisenberg antiferromagnet has been studied by Cieplak et al. [42]. We choose for our simulation the values of coupling constant and anisotropy coefficient already used by these authors for their study, i.e. $J = -1$ and $D = -0.2$; the simulation was performed on a sample of 150 spins of amplitude $S = 1$. With these values the critical fields for hysteresis are equal to $H_1 = 1.08$ (decreasing field) and $H_2 = 1.33$ (increasing field) as calculated by Cieplak, and the saturation occurs at $H_3 = 3.6$.

We present in fig. 9 the results of our simulation (magnetization curves) for this system at different temperatures. We notice the very good agreement, at low temperature ($T = 5 \times 10^{-3}$), with the calculated values of critical fields (at $T = 0$). At higher T , one observes first the narrowing of the hysteresis cycle ($T = 10^{-2}$) then its vanishing ($T = 5 \times 10^{-2}$) and the smearing out of the transition (1st order to 2nd order) ($T = 10^{-1}$).

The second example is less trivial and corresponds to the XY anisotropic triangular lattice with antiferromagnetic interactions (AFT model). A complete study of the Heisenberg anisotropic AFT model under applied field (suitable to the XY AFT model) has been performed by Miyashita [43] both analytically (ground states) and by Monte Carlo simulation (evolution with temperature). This study involved both anisotropic coupling and single ion anisotropy. In order to test the validity of the field implementation in our program and the accuracy of anisotropic coupling constants, we have undertaken a simulation of the system with the analytical results of Miyashita as reference. Our simulation was performed on an elementary sample of 3 spins in order to reproduce exactly the analytical conditions, at temperature $T = 5 \times 10^{-4}$. The field/anisotropy space was mapped with a mesh of 0.1 in field and 0.1 in anisotropy except in

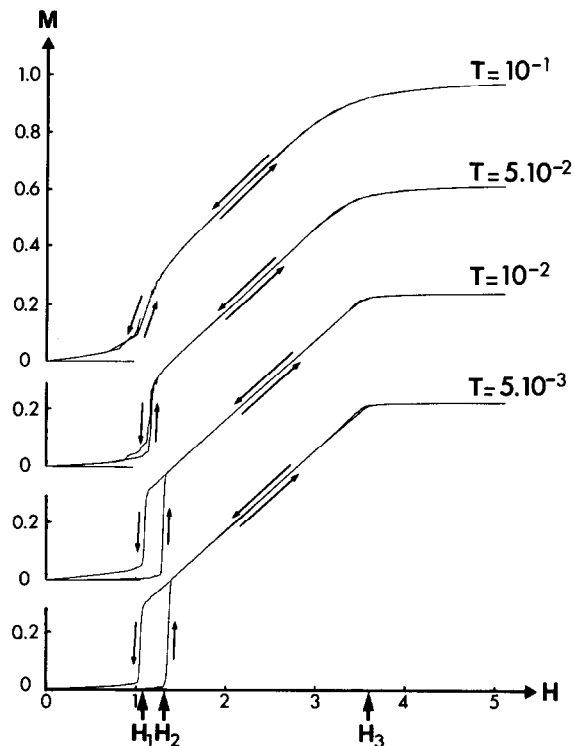


Fig. 9. Magnetization versus applied field during the simulation of the 1D Heisenberg AF model at various temperatures. H_1 , H_2 and H_3 are the transition fields determined analytically for this system [42].

the vicinity of the hysteresis where the mesh was lowered to 0.01 and 0.05, respectively. 30000 Monte Carlo cycles were performed at each point (the 10000 first ones omitted). Our results are in very good agreement with the previous one concerning the anisotropic coupling part and we shall not detail the results any further. However, our results with the single ion anisotropy model differs slightly from those presented by Miyashita. They are both summarized in fig. 10, where d denotes the anisotropy coefficient and h the applied field amplitude along the anisotropy axis (for sake of comparison we have adopted the notation of Miyashita for d and h , i.e. $d = -D$ where D is our anisotropy coefficient as defined in section 2.2 and $h = H$ defined in section 2.2 = $H/3$ in Miyashita's paper). Four ground states may be isolated which have been called a, b, d, and e in ref. [43] (schematized in fig. 10). Our results con-

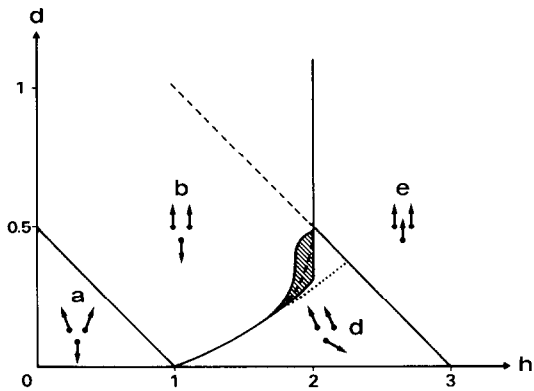


Fig. 10. Calculated phase diagram (h, d) of the XY anisotropic AFT model under applied field at $T = 5 \times 10^{-4}$. The hatched area denotes occurrence of hysteresis. The broken lines correspond to the analytical results presented by Miyashita [43]. The dotted line is the trace of the analytical calculation for the transition $b \leftrightarrow d$ with $d < d_c \approx 0.15$. a, b, d and e are the notation of the different spin configurations in ref. [43].

cerning the transitions $a \leftrightarrow b$, $d \leftrightarrow e$ and $b \leftrightarrow d$ for low anisotropy are identical to the analytical ones. They disagree about transitions $b \leftrightarrow e$, and $b \leftrightarrow d$ for strong anisotropy values, which correspond to the first order transitions of the system (Miyashita

results are indicated by broken lines in fig. 10). In our simulation the transition $b \leftrightarrow e$ is found to be independent of the strength of anisotropy and always occurs at $h = 2$; this is at variance from Miyashita's results which show a dependence of the form $h = 3 - 2d$. We also found evidence of hysteresis around the $b \leftrightarrow d$ transition for high values of d ($d > d_c \approx 0.15$), a point which had not been noticed by Miyashita. We have to mention that the metastable transition $b \leftrightarrow d$ we observe upon increasing field fits well, for $h < 2$, to the equation of the stable transition determined by this author for weak anisotropy (see fig. 10). No hysteresis was found at the $b \leftrightarrow e$ transition. The apparently quick decrease of hysteresis loop with temperature could possibly explain that this behaviour was not noticed by Miyashita.

Our last example corresponds to the square planar lattice with unequal AF interactions (we shall examine the thermal behaviour of such a system in the next section). The unit cell contains 4 atoms numbered 1 to 4 (see insert in fig. 11). Spin 1 interacts with its 4 neighbours via weak AF coupling constants ($J_1 = -0.1$ K); all three others are strongly coupled with each others ($J_2 = -10$ K). In this model the nature of interactions in-

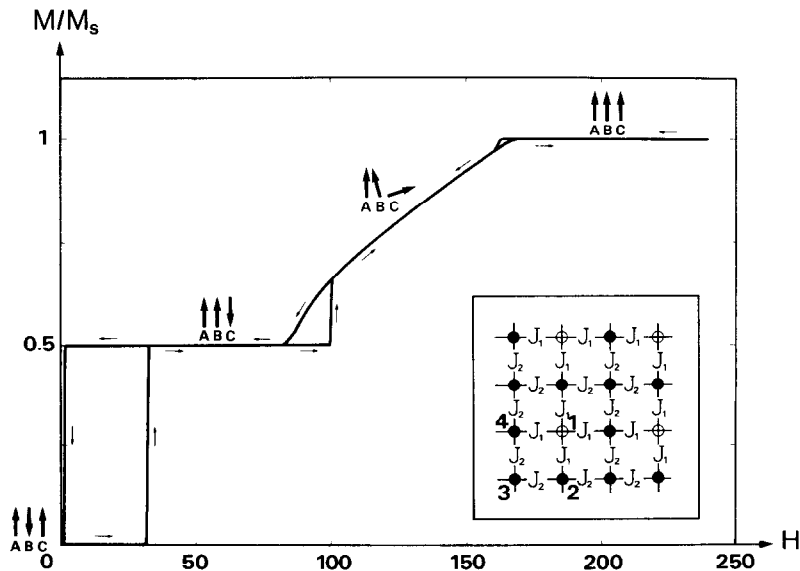


Fig. 11. Evolution of the magnetization along the applied field in the square lattice with unequal AF interactions (presented in insert) as simulated by MCMAG. The three spins schematize the sublattices A, B and C, respectively.

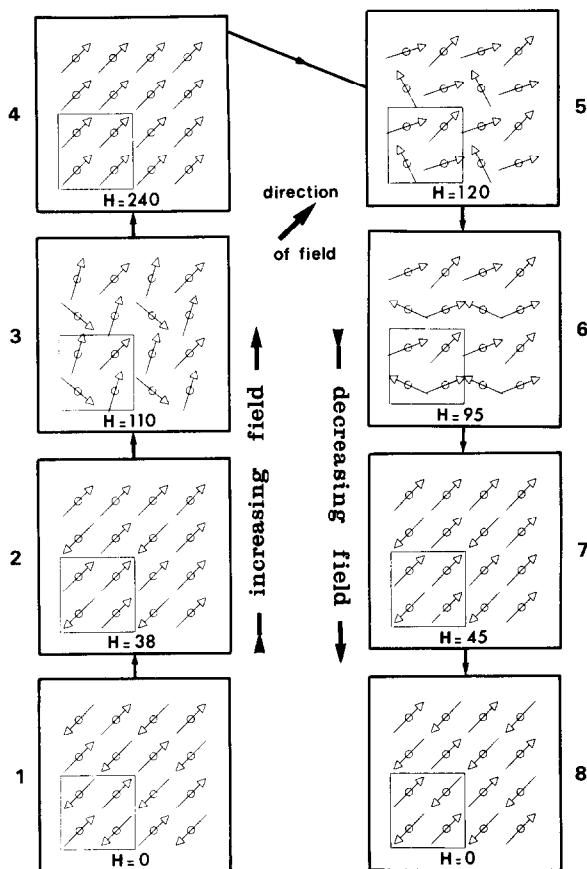


Fig. 12. Spin configurations during the simulation of the square lattice with unequal AF interactions under applied field.

induces 3 different spin sublattices called A, B and C:

- sublattice A is formed of spins of type 1, in weak interaction with surrounding spins (4×0.1 K),
- sublattice B is built up of spins 2 and 4, which undergo 2 weak and 2 strong interactions with their neighbours (2×0.1 K + 2×10 K),
- sublattice C is formed of spins 3 which are strongly correlated (4×10 K).

The anisotropy coefficient $D = -2$ K is strong compared to the weak interactions (-0.1 K) but weak compared to the strong ones (-10 K). This point must be responsible for a peculiar behaviour under magnetic field, that we have studied with the program. The steps of the process are il-

lustrated by the corresponding spin arrangement in fig. 12. The field was applied along the direction of anisotropy of sublattice A, and progressively increased then decreased. Fig. 11 shows the evolution of magnetization in the direction of field during this process, together with a schematic representation of the relative configuration of the three sublattices. The first transition is of the metamagnetic type, with an abrupt reversal of sublattices B and C toward sublattice A, which stays along the field direction (fig. 12-2). This is a consequence of the weak coupling of spin 1 with neighbouring spins (namely sublattice B) compared to the strong anisotropy. We have already mentioned that in this case, a metamagnetic transition occurs. Coupling between sublattices B and C remains unchanged. The second transition (fig. 12-3) concerns sublattices B and C and is of spin-flop type, owing to the strong exchange between these sublattices compared to the anisotropy. Until saturation (fig. 12-4) the angle between spins of sublattice B and field is smaller than the angle of sublattice C with field (sublattice B contains twice as many spins than sublattice C).

Upon decreasing field we notice the occurrence of two hysteresis cycles (fig. 11). In the vicinity of the high field transition, the change from a canted configuration of spins to the collinear one is continuous. The hysteresis at the metamagnetic transition is a consequence of the alignment of the applied field along the direction of spins 1, the less strongly coupled sublattice. The energy necessary to reverse this sublattice is smaller and the transition takes place at a lower field. The zero-field configuration is the opposite of the starting configuration.

3.5. Dynamical behaviour with temperature

All previous applications have been restricted to very low temperatures, the “cooling” of the sample being only a technical trick (simulated annealing) to obtain the ground state configuration of the system, starting from complete disorder. In principle, the use of a proper Hamiltonian for a given system should allow to determine its ordering temperature [44]. A method to locate the phase transitions would be to calculate the free

energy F of the system. However, the important sampling method of Metropolis yields estimates of extensive quantities such as internal energy E and magnetization but does not give directly any information on the entropy S nor on the free energy of the system $F = E - TS$. This results from the fact that entropy is a function of the unknown probability with which the configurations of the system are generated. This problem has received considerable attention in the literature and various methods have been suggested (see for instance refs. [45–49]). However, most of these methods are somewhat unpractical or rather computer time consuming and have not been implemented yet in MCMAG.

Another (technical) problem arises from the limitations of the computer; indeed, calculations are performed for systems of finite size and it has long been known that reliable information from Monte Carlo work on the behaviour of an experimental (infinite) system is obtained only if the effect of the sample size is carefully considered [50]; for instance, in the case of the simple-cubic Ising lattice, it has been shown [51] that the ordering temperature has an asymptotic dependence on the sample dimension (finite edges and periodic boundary conditions lead to different asymptotic behaviours); one may also expect the topology of the lattice and the values of the coupling constants to influence this behaviour. Generally speaking, the use of small simulation box smears out the ordering transition and shifts the temperature.

For the kind of applications considered in this paper, an additional difficulty arises from the limited information usually available about the values of the coupling constants and anisotropy coefficients; moreover, when available in the literature, these parameters have been determined at a single (usually low) temperature although they may vary noticeably with temperature, as evidenced in a few systems (see for instance refs. [52–54]). This possible variation of the exchange and anisotropy parameters is not taken into account in the current version of the program.

Although the program MCMAG can in principle perform simulation of fairly large lattices, our aim was essentially to provide a tool to help at determining or predicting real magnetic structures

which can be achieved by working with fairly small (and inexpensive) simulation samples. As a consequence, these calculations will only yield qualitative information on the temperature dependent behaviour of the sample (in particular, the sample behaviour in the vicinity of a phase transformation must be considered with caution). In spite of this limitation, such simulations can be used to account for dynamical effects encountered during thermal ordering. This aspect will be illustrated in this section by three examples, taken from results of our laboratory.

The first one concerns the above example of $\text{Ba}_2\text{Ni}_3\text{F}_{10}$ for which it can be seen from simulated susceptibility curve (fig. 13a) that the calculated ratio $T_N/\theta_p = -0.62$ is close to the experimental one (-0.71). The simulated specific heat curve is shown in fig. 13b.

The second example is concerned with the influence of topological frustration on ordering temperature. It has already been pointed out, both experimentally [55] and analytically [56–58] that magnetic frustration lowers the critical temperature. A very good illustration is provided by the polymorphism of iron III fluoride. Under appropriate synthesis conditions, FeF_3 crystallizes with three different forms: a distorted perovskite, an hexagonal tungsten bronze structure type (H.T.B.) and a pyrochlore type [59,60]. All of them are essentially antiferromagnets (the perovskite form of FeF_3 is a weak ferromagnet) with drastically different Néel temperatures for the perovskite form orders at 365 K, the H.T.B. form at 110 K and the pyrochlore form below 20 K [55]. The superexchange Fe–F–Fe angle decreases slightly [55] from the perovskite (152.15°) to the pyrochlore structure (141.65°), but this variation is by far too small to explain such differences. The examination of Fe^{3+} subnetworks (fig. 14 left part) shows that the high T_N form is built up from unfrustrated square platelets, while H.T.B. form exhibits both square and triangular platelets and pyrochlore form only frustrated triangular platelets. Thus the frustration rate grows from high T_N to low T_N form and frustration is believed to be a likely explanation for the lowering of ordering temperature.

We have undertaken a magnetic Monte Carlo

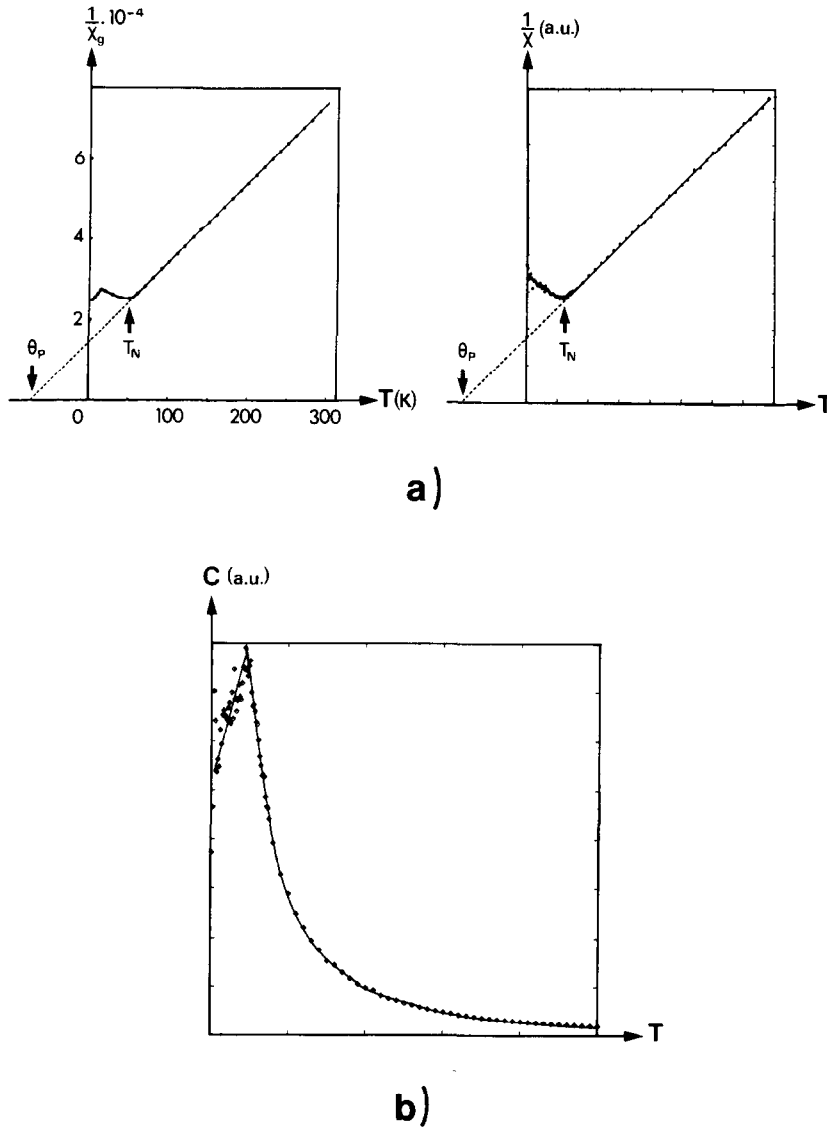


Fig. 13. (a) Experimental reverse susceptibility curve versus temperature for $\text{Ba}_2\text{Ni}_3\text{F}_{10}$ (left, from ref. [17]) compared to the simulated one (right); (b) simulated specific heat curve versus temperature for $\text{Ba}_2\text{Ni}_3\text{F}_{10}$. Simulation parameters: sample: $1 \times 1 \times 2$ cells (24 spins); periodic boundary conditions; 30000 Monte Carlo cycles per spin at each temperature, the 10000 first ones omitted for the mean values calculation.

simulation of the three forms of FeF_3 in order to assess the validity of the previous argument. The samples used for simulation were built up from 48 atoms for each form. All (nearest neighbour) interactions were set to the same (negative) value; to test the only influence of topological frustration the spin amplitudes were also kept equal (in fact

magnetic moments also undergo a substantial reduction in the frustrated forms). Periodic boundary conditions were applied on all three samples. The results of simulation are presented in the right hand part of fig. 14. The evolution of the resultant magnetic moment of an iron (III) site is plotted versus temperature for each structure. The dif-

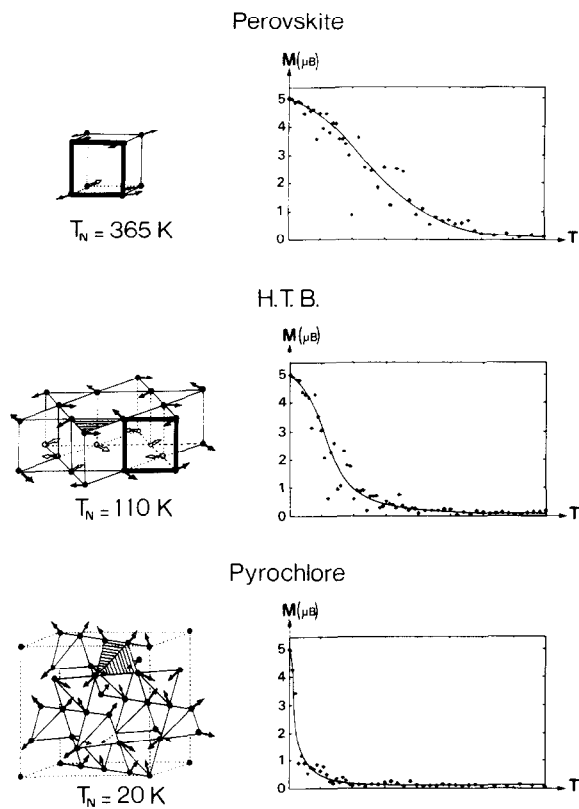


Fig. 14. Correlation between ordering temperature and frustration in the three crystalline forms of Fe_3 . The left part of the figure provides a description of the Fe^{3+} sublattice of each structure where non-frustrated (heavy lines) and frustrated (hatched) cycles are outlined (from ref. [55]). The right part of the figure gives Monte Carlo results of the temperature dependence of the magnetic moment of one site during the cooling, with the same temperature scale for each form. Simulation parameters (for each structure): sample of 48 spins; 15000 MC cycles per spin at each temperature from which the 5000 first ones were omitted in statistics; periodic boundary conditions.

ference between ordering temperatures is at least very large; it unambiguously shows that frustrating topology is the main responsible for this effect.

A third example is provided by the fluoride NaMnFeF_6 , which crystallizes in a trigonal cell ($a = 9.041(2) \text{ \AA}$, $c = 5.004(2) \text{ \AA}$) [61]. The stacking of atoms in term of coordination polyhedra is shown in fig. 15. The magnetic ordering takes place below $T_N = 45 \text{ K}$. A spontaneous magnetization appears during cooling, which exhibits a peculiar curvature [62], passing through a maxi-

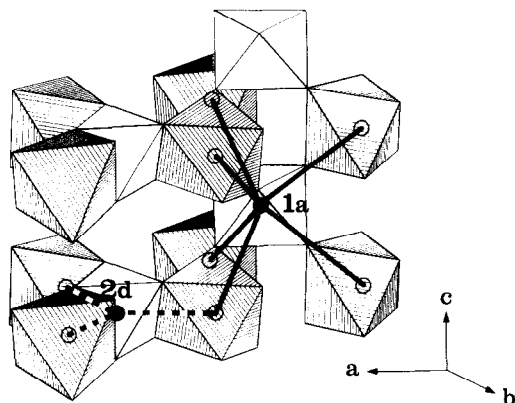


Fig. 15. The crystal structure of NaMnFeF_6 (from ref. [61]). Hatched octahedra surround Mn^{2+} . Two Fe^{3+} sites (1a and 2d) are present as well as two different coupling constants $J_{180^\circ}(\text{Mn}-\text{Fe})$ (—) and $J_{90^\circ}(\text{Mn}-\text{Fe})$ (---).

um value at about 32 K and decreasing to zero at lower temperature (fig. 16b left). This evolution is confirmed by Mössbauer measurements: the hyperfine fields variation versus temperature shows that the moment of Fe(2d) site saturates at a lower temperature than Fe(1a) (fig. 16a left). This effect has been referenced to as “soft spin” behaviour. At low temperature the magnetic structure is that of a classical antiferromagnet, with magnetic moments of Fe^{3+} cations oriented antiparallel to the Mn^{2+} ones, along the c axis [63].

Clearly NaMnFeF_6 is not submitted to any magnetic frustration. The two nearest neighbour interactions (between Mn^{2+} and Fe^{3+}) are underlined in fig. 15. One involves a 90° d^5-d^5 superexchange mechanism, while the other follows a 180° superexchange path. Kanamori–Goodenough rules predict that the first one must be weaker than the second. An explanation of the magnetic behaviour of NaMnFeF_6 could be the unbalanced values of these interactions. We tried to shed light on this point by simulating the magnetic behaviour of this compound with MCMAG. In agreement with Kanamori–Goodenough rules, $J_{180^\circ}(\text{Mn}-\text{Fe})$ was set to -3 K and $J_{90^\circ}(\text{Mn}-\text{Fe})$ to -0.5 K . Results are given in fig. 16 (right parts). Magnetic moments of 1a and 2d sites show a simulated evolution versus temperature very similar to the experimental one, as does

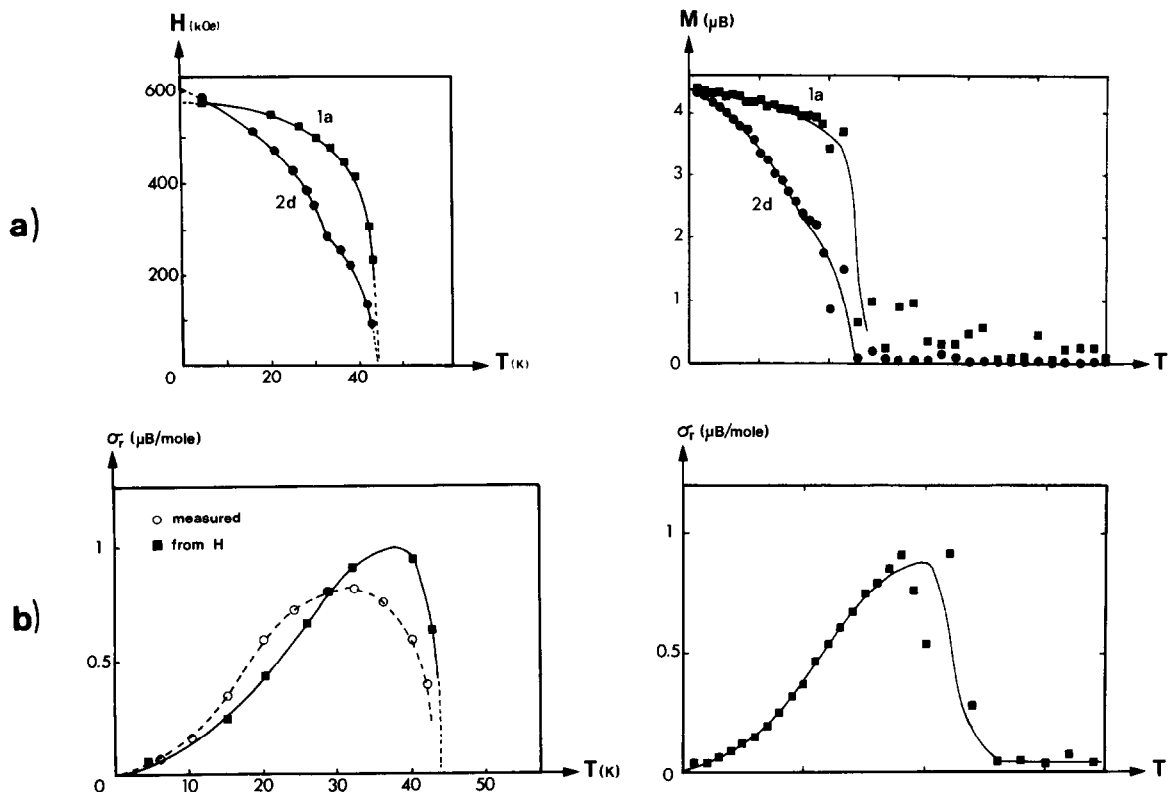


Fig. 16. (a) Hyperfine fields at Fe(1a) and Fe(2d) in NaMnFeF_6 (taken from ref. [63]) (left) compared to the magnetic moments as simulated by MCMAG (right); (b) measured and calculated spontaneous magnetization in NaMnFeF_6 (left) compared to the Monte Carlo result (right).

the remanent magnetization. Therefore no additional hypothesis than the commonly accepted ones appears to be needed to explain this “soft spin” behaviour.

A more pronounced effect has been simulated with a topology corresponding to the compound $\beta\text{-LiMnFeF}_6$, which undergoes an “idle spin” behaviour [64]. We illustrate this behaviour with the simple 2D square model with unequal AF interactions, which has been investigated under magnetic field in the previous section. In this example, the coupling constant between spin 1 and its neighbours is an hundred times weaker than the coupling constants connecting other spins. In such

a system, it appears that sublattices have different ordering temperatures (fig. 18): the sublattice 1 orders at a lower temperature than the three others (fig. 17). A similar phenomenon occurs in $\beta\text{-LiMnFeF}_6$. These results emphasize the assumption that differences of magnitude between exchange integrals may be, in some cases, the origin of departure in magnetic subnetwork saturation.

In conclusion to this section, we can point out that, even if the absolute determination of ordering temperature is usually not possible, the above examples show that the program can efficiently reproduce the qualitative behaviour of a magnetic structure upon cooling.

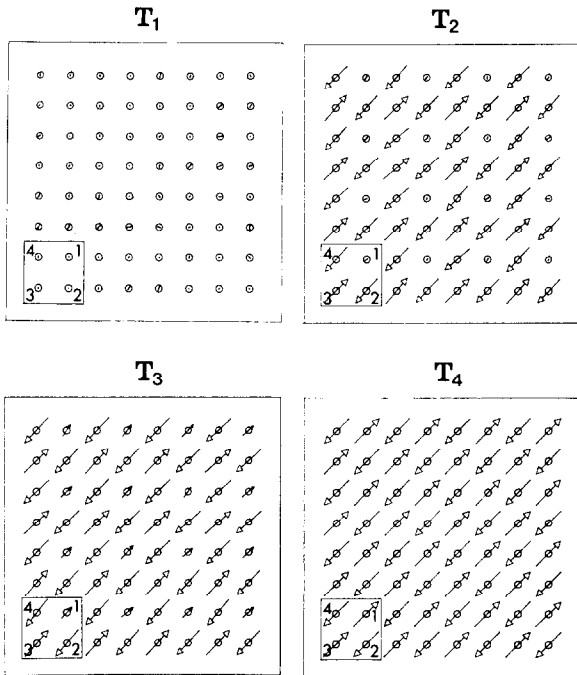
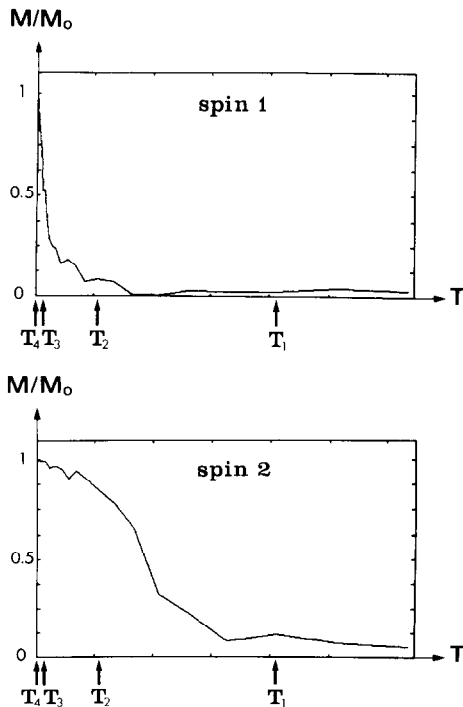


Fig. 17. Monte-Carlo simulation results of the square lattice with unequal AF interactions ("idle spin" behaviour). Spin 1 is weakly coupled with its neighbours. The four views correspond to the temperatures noted by arrows in fig. 18.



4. Conclusion

The main advantage of this program is its ability to accept any kind of 1D, 2D or 3D topology provided that it presents a periodic or cluster arrangement. The absence of limitation in interacting distance should allow to study complicated systems. The actual form of the Hamiltonian is quite simple, but more sophisticated formula could easily be introduced without changing the general structure of the program. As a future development, random or distributed exchange integrals could be introduced in order to simulate spin glass behaviour on any kind of topology, as well as local modification of some integrals to test the influence of impurities in a sample.

Over the past years, special attention has been focussed on model calculation of coupling constants in solids, based upon geometrical consideration [11,30]. In a first step, the program could provide an opportunity to test the validity of these models in non trivial cases (i.e. when competing interactions occur). A more advanced stage, and perhaps more Utopian view, would be the direct simulation of magnetic structures from crystallographic data only.

Acknowledgements

The authors would like to express their special thanks to Professor G. Ferey and Dr. M. Goldmann for helpful discussions, to Dr. M. Guillot for complementary magnetic measurements and to Dr. P.J. Brown for critical reading of the manuscript.

Fig. 18. Effective moment of spin 1 and spin 2 during the cooling of the square lattice model with unequal AF interactions. Spin 1 orders at a lower temperature than spin 2 ("idle spin" behaviour). The arrows indicate the four temperatures corresponding to the configurations drawn in fig. 17.

Appendix A. Description of an input file for MCMAG

The input parameters are defined as follows:

NA	total number of magnetic atoms in the sample cell	D	anisotropy coefficient for the spin of atom NAT
JCOD	code for interactions: JCOD = 0 for isotropic interactions JCOD = 1 for anisotropic interactions	Dx, Dy, Dz	direction of the anisotropy for spin NAT
NM	number of formula units per cell (only to scale results to mole units)	NAV	index of a neighbour of atom NAT
NAT	index of a given atom	Av, Bv, Cv	relative coordinates of the cell in which atom NAV is located (0, 0, 0 = basic unit cell)
NV	total number of neighbours of the atom NAT	J	value of the isotropic interaction J(NAT, NAV) in kelvin
		Jx, Jy, Jz	components of the anisotropic interaction J(NAT, NAV) in kelvin
		NI, NF, S	amplitude of the spins of atom number NI to NF is equal to S ($NF \leq NA$)
		A, B, C	unit cell lengths
		AA, AB, AG	unit cell angles

The input file cards are the following:

CARD	FORMAT	PARAMETERS
TITLE CARD	20A4	
DEFINITION CARD	free	NA, JCOD, NM
ATOM CARD	free	NAT, NV, D, Dx, Dy, Dz
INTERACTION CARD	free	NAV, Av, Bv, Cv, J if JCOD = 0 NAV, Av, Bv, Cv, Jx, Jy, Jz if JCOD = 1
SPIN CARD	free	NI, NF, S
CELL CARD	free	A, B, C, AA, AB, AG

Table 1 provides a simple example of input file, according to the illustration of fig. 1.

Appendix B. Technical details

The program is written in Fortran 77 language and has been developed on the central computer VAX-8650 of the Institut Laue Langevin (Grenoble, France). Random numbers are generated by the random number generator of the computer and by the subroutine RAN3D of the mathematical library of the CERN, which provide random points at the surface of a sphere. The memory size requested by the program is highly dependent on the upper limit of sample size. It may be very

roughly expressed as $50 + 0.082N$ kbytes, where N is the maximum number of spins in a sample. The CPU time per Monte Carlo step is dependent not only on the sample size, but also on the number of neighbours per spin. As an indication, we give the calculation time required for two examples presented in this paper. One thousand Monte Carlo steps request on the VAX-8650:

- 3.3 s of CPU time for a sample of $1 \times 1 \times 2$ cells of $Ba_2Ni_3F_{10}$ (i.e. 24 spins, each of them with 4 to 6 neighbours)
- 101 s of CPU time for a sample of $3 \times 3 \times 21$ cells of $\beta\text{-MnO}_2$ (i.e. 378 spins, each of them with 14 neighbours).

The program is available from the authors on request.

References

- [1] K. Binder and D. Stauffer, in: *Applications of the Monte Carlo Method in Statistical Physics*, ed. K. Binder (Springer-Verlag, Berlin, 1984) p. 1.
- [2] K. Binder, in: *Monte Carlo Methods in Statistical Physics*, ed. K. Binder (Springer-Verlag, Berlin, 1979) p. 1.
- [3] D.P. Landau, in: *Monte Carlo Methods in Statistical Physics*, ed. K. Binder (Springer-Verlag, Berlin, 1979) p. 121.
- [4] N. Metropolis, A.W. Rosenbluth, M.N. Rosenbluth, A.H. Teller and E. Teller, *J. Chem. Phys.* 21 (1953) 1087.
- [5] S. Kirkpatrick, C.D. Gellatt Jr. and M.P. Vecchi, *Science* 220 (1983) 671.
- [6] K.W.H. Stevens, in: *Magnetism*, eds. G.T. Rado and H. Suhl (Academic Press, New York, London, 1963) p. 1.
- [7] S. Fujiki, K. Shutoh, Y. Abe and S. Katsura, *J. Phys. Soc. Japan* 52 (1983) 1531.
- [8] S. Katsura, T. Ide and T. Morita, *J. Stat. Phys.* 42 (1986) 381.
- [9] J. Kanamori, *J. Phys. Chem. Solids* 10 (1959) 87.
- [10] J.B. Goodenough, *Magnetism and the Chemical Bond* (Wiley Interscience, New York, 1963).
- [11] L.J. De Jongh and R. Block, *Physica* 79B (1975) 568.
- [12] L. Jansen and R. Block, *Physica* 86–88B (1977) 1012.
- [13] D.J. Newman, *Physica* 86–88B (1977) 1018.
- [14] N. Fuchikami, *Physica* 115B (1983) 219.
- [15] E.L. Bominaar and R. Block, *Physica* 121B (1983) 109.
- [16] E.L. Bominaar and R. Block, *Phys. Rev.* B33 (1986) 3672.
- [17] M. Leblanc, G. Ferey and R. De Pape, *J. Solid State Chem.* 33 (1980) 317.
- [18] P. Lacorre, J. Pannetier and G. Ferey, *J. Magn. Magn. Mat.* 66 (1987) 213.
- [19] M.T. Hutchings, M.F. Thorpe, R.J. Birgeneau, P.A. Fleury and H.J. Guggenheim, *Phys. Rev.* B2 (1970) 1362.
- [20] S.R. Chinn, H.J. Zeiger and J.R. O'Connor, *Phys. Rev.* B3 (1971) 1709.
- [21] J. Als-Nielsen, R.J. Birgeneau and H.J. Guggenheim, *Phys. Rev.* B6 (1972) 2030.
- [22] J. Skalyo Jr., G. Shirane, R.J. Birgeneau and H.J. Guggenheim, *Phys. Rev. Lett.* 23 (1969) 1394.
- [23] G. Toulouse, *Commun. Phys.* 2 (1977) 115.
- [24] L.G. Marland and D.D. Betts, *Phys. Rev. Lett.* 43 (1979) 1618.
- [25] T. Oguchi, H. Nishimori and Y. Taguchi, *J. Phys. Soc. Japan* 55 (1986) 323.
- [26] S.E. Korshunov and G.V. Uimin, *J. Stat. Phys.* 43 (1986) 1.
- [27] P. Lacorre, M. Leblanc, J. Pannetier and G. Ferey, *J. Magn. Magn. Mat.* 66 (1987) 219.
- [28] J.C. Dewan and A.J. Edwards, *J. Chem. Soc. Chem. Commun.* (1977) 533.
- [29] a) A.J. Edwards, private communication.
b) J.C. Dewan, A.J. Edwards and J.J. Guy, *J. Chem. Soc. Dalton Trans.* 12 (1986) 2623.
c) D. Kissel and R. Hoppe, *Z. Naturforsch.* 42b (1987) 135.
- [30] G.A. Sawatzky and F. Van der Woude, *J. de Phys. Colloq.* 12 (1974) C6–47.
- [31] A. Yoshimori, *J. Phys. Soc. Japan* 14 (1959) 807.
- [32] J.A. Gonzalo and D. Cox, *An. Fis. (Spain)* 66 (1970) 407.
- [33] N. Ohama and Y. Hamaguchi, *J. Phys. Soc. Japan* 30 (1971) 1311.
- [34] J. Baruchel, S.B. Palmer and M. Schlenker, *J. de Phys.* 42 (1981) 1279.
- [35] Y. Laligant, J. Pannetier, M. Leblanc, P. Labbé, G. Heger and G. Ferey, *Z. Krist.* (in press).
- [36] Y. Laligant, J. Pannetier and G. Ferey, *J. Solid State Chem.* 66 (1987) 242.
- [37] Y. Laligant, private communication. The N.D. magnetic moments correspond to the results of refinement considering the true space group Pnma, as determined in ref. [35] (to be published).
- [38] Y. Laligant, Y. Calage, E. Torres-Tapia, J.-M. Grenèche, F. Varret and G. Ferey, *J. Magn. Magn. Mat.* 61 (1986) 283.
- [39] M. Guillot, private communication.
- [40] E. Strykowski and N. Giordano, *Advan. Phys.* 26 (1977) 487.
- [41] L. Néel, *Procès Verbal Xième Conseil de Physique Solvay* (1954) 251.
- [42] M. Cieplak, G. Ismail and J. Lusakowski, *J. Phys.* C20 (1987) 1301.
- [43] S. Miyashita, *J. Phys. Soc. Japan* 55 (1986) 3605.
- [44] K.A. Gehring, M.J.M. Leask and J.H.M. Thornley, *J. Phys.* C2 (1969) 484.
- [45] Z.W. Salsburg, J.D. Jacobson, W. Fickett and W.W. Wood, *J. Chem. Phys.* 30 (1959) 65.
- [46] J.P. Valteau and D.N. Card, *J. Chem. Phys.* 57 (1972) 5457.
- [47] Z. Alexandrowicz, *J. Stat. Phys.* 14 (1976) 1.
- [48] H. Meirovitch, *Chem. Phys. Lett.* 45 (1977) 389.
- [49] K. Binder, *Z. Phys.* B45 (1981) 61.
- [50] K. Binder, *Advan. Phys.* 23 (1974) 917.
- [51] D.P. Landau, *Phys. Rev.* B14 (1976) 255.
- [52] P. Escudier, *Thèse de Doctorat, Université Scientifique et Médicale de Grenoble, France* (1973).
- [53] S. Hirose, Y. Matsuura, H. Yamamoto, S. Fujimura, M. Sagawa and H. Yamauchi, *J. Appl. Phys.* 59 (1986) 873.
- [54] Z. Drzazga and M. Drzazga, *J. Magn. Magn. Mat.* 65 (1987) 21.
- [55] G. Ferey, R. De Pape, M. Leblanc and J. Pannetier, *Rev. Chim. Min.* 23 (1986) 474.
- [56] P. Hoever, W.F. Wolff and J. Zittartz, *Z. Phys.* B41 (1981) 43.
- [57] G. Sun and T. Oguchi, *J. Phys. Soc. Japan* 55 (1986) 3117.
- [58] I.R. McLennaghan and D. Sherrington, *J. Phys.* C20 (1987) 1701.
- [59] M. Leblanc, R. De Pape and G. Ferey, *Solid State Commun.* 58 (1986) 171.
- [60] R. De Pape and G. Ferey, *Mater. Res. Bull.* 21 (1986) 971.
- [61] M. Leblanc, *Thèse de Doctorat, Université du Maine, France* (1984).
- [62] M. Tamine, Y. Calage, M. Leblanc, G. Ferey and F. Varret, *Hyperfine Interactions* 28 (1986) 529.
- [63] G. Courbion and M. Leblanc, private communication (to be published).
- [64] G. Courbion, R. De Pape, J. Teillet, F. Varret and J. Pannetier, *J. Magn. Magn. Mat.* 42 (1984) 217.